Time-dependent flow across a step: the slip with friction boundary condition

Volker John[1,‡] and Anastasios Liakos[2,*,†]

[1]*FR 6.1-Mathematik, Universität des Saarlandes, Postfach 15 11 50, 66041 Saarbrücken, Germany*
[2]*Department of Mathematics, U.S. Naval Academy, Annapolis MD 21402, U.S.A.*

SUMMARY

The paper studies numerically the slip with friction boundary condition in the time-dependent incompressible Navier–Stokes equations. Numerical tests on two- and three-dimensional channel flows across a step using this boundary condition on the bottom wall are performed. The influence of the friction parameter on the flow field is studied and the results are explained according to the physics of the flow. Due to the stretching and tilting of vortices, the three-dimensional results differ in many respects from the two-dimensional ones. Copyright © 2005 John Wiley & Sons, Ltd.

KEY WORDS: Navier–Stokes equations; slip with friction boundary conditions; flow across a step

1. INTRODUCTION

The numerical solution of the Navier–Stokes equations with no-slip boundary conditions has been studied exhaustively (see References [1–3]). The term *no-slip* pertains to the fact that the fluid adheres to the boundary of the flow domain. The no-slip condition is widely accepted as a correct boundary condition for moderate fluid velocities and stresses. Its acceptance, as Day [4] and LeRoux [5] state, is due to:

- comparisons between experimental and theoretical solutions of flow problems with small fluid velocities;
- direct observations of fluids with moderate velocities near surfaces, and more recently
- comparisons between numerical simulations and experimental results of a large array of flow problems, but again only for moderate velocities.

---

*Correspondence to: A. Liakos, Department of Mathematics, U.S. Naval Academy, Annapolis MD 21402, U.S.A.
†E-mail: liakos@usna.edu
‡E-mail: john@math.uni-sb.de

Another argument in favour of the no-slip condition (compared to the partial slip laws) is its mathematical convenience (e.g. validity of the Poincaré–Friedrichs' inequality).

Naturally, there are exceptions to the no-slip rule. Investigations of slip flow were first presented by Kundt and Warburg [6], who found that the discharge of gas from a tube at low density was larger than that calculated for the same pressure difference assuming laminar flow. These experiments led Maxwell to determine the boundary conditions at the wall from a consideration of the interaction of gas molecules with the surface of a solid body [7]. He found that the tangential velocity at the surface was small but finite and that slip flow could occur. Finally, Petroff [8] suggested that slipping occurs at very high speeds with a substance that is a good lubricant.

Another example, where the imposition of the no-slip boundary condition might be inappropriate, is high Reynolds number flow. As the Reynolds number increases, the stress in the system becomes higher. Once it surpasses a given value, the fluid slips along the boundary. Slip is the physical mechanism with which the fluid relieves the stress. Thus, we expect that, for higher Reynolds numbers, the flow at the boundary satisfies a slip with friction condition. The numerical simulation of high Reynolds number flows requires the use of a turbulence model. Currently, one of the most promising approaches for modelling turbulence is large eddy simulation (LES). The LES seeks to compute the large eddies of a turbulent flow accurately while the influence of the small flow structures onto the large ones is modelled. Galdi and Layton [9] propose to apply slip with friction and no penetration boundary conditions for the large eddies. Such boundary conditions are more suitable than no-slip boundary conditions to describe phenomena which can be observed in nature, e.g. the main vortices of a hurricane do not stick at the boundary therefore the no-slip law is not satisfied. These vortices move on the boundary (slip), losing energy while moving (friction), and do not penetrate the boundary.

Navier [10] proposed a *partial slip* boundary condition which admits linear friction. Specifically, slip occurs in the opposite direction as the resistive force the wall exerts on the fluid; in addition, there is a *linear* resistance to slip. If the friction coefficient is a function of the thermodynamic variables (in particular if $\beta = \infty$ in (1) below, except at low pressures), then the slip with linear friction boundary condition can even account for adherence [11].

The condition of no slipping at the boundary has been dropped by Duhem [12, 13] and later by Oseen [14]. In particular, Duhem's boundary conditions (in channel flow with one part of the boundary moving with a constant velocity) allow for adherence when the coefficient of friction was larger than a constant times the velocity of the wall, and slipping in the opposite case. A theory of resistance based upon the idea of kinematic viscosity and thermal conductivity which vary with the velocity was first proposed by Noaillon [15]. His boundary condition implies adherence for low tangential stresses and high pressures and reduces to the slip with friction boundary conditions for the opposite extremes.

The time-dependent Navier–Stokes equations with Navier's slip boundary conditions has been studied analytically by Clopeau *et al.* [16], and Coron [17]. The former have exhibited existence of the regular solutions for the 2-D Navier–Stokes equations with smooth compatible data. The latter have exhibited existence of solutions for the 'controlled' 2-D, time-dependent Navier–Stokes equations with Navier's slip law on a part of the boundary. That is, given initial data, test whether there exist solutions to the Navier–Stokes equations which, for a fixed time, are 'arbitrarily' close to a given flow field.

To the knowledge of the authors, there are only few numerical studies of the slip with friction boundary condition. Therefore, a systematic study of the effects of this boundary condition in well-defined test problems is essential. We have chosen to use the flow across a step since recirculation of a flow is a very natural situation. Applications of the study herein include 'wind engineering and many fluid devices, such as weirs, gas turbines, turbo machines and combustion ducts' [18]. More motivation for the choice of this test problem is given at the beginning of Section 3. Our plan is to study the influence of the friction on the reattachment points (in 2-D) and isolines (in 3-D) of recirculating vortices behind the step for three types of flows:

- stationary flows;
- time-dependent laminar flows; and
- turbulent flows.

The studies for the stationary flow can be found in Reference [19]. Their results are summarized in the description of the test problems, Remarks 1 and 2. The current work contains the study of time-dependent laminar flows. The motivation for choosing this type of flows as the second step in our study comes from the fact that such flow problems can be discretized by a Galerkin finite element method for the Navier–Stokes equations. This will not be possible for turbulent flows since a direct numerical simulation (DNS) by a Galerkin finite element discretization seeks to simulate the behaviour of all persisting scales. The smallest scales in turbulent flows, the so-called Kolmogorov scales, are much smaller than the grid size which can be afforded on present day computers, e.g. see Reference [20]. Thus, the small scales cannot even be represented on such meshes. However, these scales are important for the physics of turbulent flows (energy cascade). It is necessary to model the influence of the unresolved scales onto the resolved ones, which implies using a turbulence model. In this situation, the evolution of the reattachment points (lines) will not only depend on the friction but most probably also on the turbulence model which is used. The results for time-dependent laminar flows may help to distinguish between both influences.

The paper is organized as follows. Section 2 introduces the Navier–Stokes equations with slip with friction boundary conditions and contains comments on their discretization. The test problems are described in Section 3. Section 4 contains the numerical results for the 2-D flow across a step and Section 5 for the 3-D flow across a step. The most important conclusions from the numerical studies are summarized in Section 6.

2. THE NAVIER–STOKES EQUATIONS WITH SLIP WITH FRICTION BOUNDARY CONDITIONS

Let $\Omega \subset \mathbb{R}^d$, $d = 2, 3$, be a bounded domain with boundary $\partial\Omega = \Gamma_{\mathrm{diri}} \cup \Gamma_{\mathrm{sf}} \cup \Gamma_{\mathrm{out}}$ such that all three parts of the boundary are mutually disjoint. The outward pointing unit normal vector on $\partial\Omega$ is denoted by $\mathbf{n}$. It is assumed that $\mathbf{n}$ exists almost everywhere on $\partial\Omega$. Throughout this paper, matrix vector notations are used, i.e. a vector $\mathbf{v}$ is always a column vector and the corresponding row vector is denoted by $\mathbf{v}^{\mathrm{T}}$.

We consider the incompressible Navier–Stokes equations in dimensionless form

$$\frac{\partial \mathbf{u}}{\partial t} - 2Re^{-1}\nabla \cdot \mathbb{D}(\mathbf{u}) + (\mathbf{u} \cdot \nabla)\mathbf{u} + \nabla p = \mathbf{0} \quad \text{in } (0,T] \times \Omega$$

$$\nabla \cdot \mathbf{u} = 0 \quad \text{in } [0,T] \times \Omega$$

$$\mathbf{u}(0,\cdot) = \mathbf{u}_0 \quad \text{in } \Omega$$

$$\mathbf{u} = \mathbf{g} \quad \text{in } [0,T] \times \Gamma_{\text{diri}} \tag{1}$$

$$\mathbb{S}(\mathbf{u},p)\mathbf{n} = \mathbf{0} \quad \text{in } [0,T] \times \Gamma_{\text{out}}$$

$$\mathbf{u} \cdot \mathbf{n} = 0 \quad \text{in } [0,T] \times \Gamma_{\text{sf}}$$

$$\mathbf{u} \cdot \boldsymbol{\tau}_k + \beta^{-1}\mathbf{n}^{\mathrm{T}}\mathbb{S}(\mathbf{u},p)\boldsymbol{\tau}_k = 0 \quad \text{in } [0,T] \times \Gamma_{\text{sf}}$$

where $1 \leqslant k \leqslant d-1$. The unknown quantities are the velocity $\mathbf{u}$ and the pressure p. The Reynolds number Re, the initial velocity $\mathbf{u}_0$, the final time T and the Dirichlet boundary conditions $\mathbf{g}$ on Γ_{diri} are prescribed. On Γ_{out}, an outflow or do-nothing boundary condition is given. Here, $\mathbb{S}(\mathbf{u},p)$ is the stress tensor

$$\mathbb{S}(\mathbf{u},p) = 2Re^{-1}\mathbb{D}(\mathbf{u}) - p\mathbb{I}$$

where $\mathbb{I}$ is the unit tensor and $\mathbb{D}(\mathbf{u})$ the velocity deformation tensor

$$\mathbb{D}(\mathbf{u}) = \frac{\nabla \mathbf{u} + \nabla \mathbf{u}^{\mathrm{T}}}{2}$$

On Γ_{sf}, slip with linear friction and no penetration boundary conditions are applied. The friction is given by the non-negative function β. In our computations, β will be piecewise constant. The tangential vectors $\boldsymbol{\tau}_k$, $1 \leqslant k \leqslant d-1$, are chosen such that $\{\mathbf{n}, \boldsymbol{\tau}_1\}$ in two dimensions and $\{\mathbf{n}, \boldsymbol{\tau}_1, \boldsymbol{\tau}_2\}$ in three dimensions build an orthonormal basis. The limit $\beta \to 0$ leads to free-slip boundary conditions and in the limit $\beta \to \infty$, the no-slip boundary condition is recovered. The value of the friction coefficient β in model situations where wall laws for the velocity have been applied is studied in Reference [21].

The Navier–Stokes equations (1) are discretized in the following way:

1. *Discretization of* (1) *in time.* In the 2-dimensional simulations, the fractional-step θ-scheme and in the 3-dimensional simulations, the Crank–Nicolson scheme are applied. Both are second-order implicit time stepping schemes. The time discretization leads in each discrete time step to a non-linear system of equations.
2. *Variational formulation and linearization.* The non-linear system of equations is reformulated as a variational problem which is linearized by a fixed point iteration.
3. *Discretization of the linear systems in space.* The linear system of equations arising in each step of the fixed point iteration is discretized by a finite element discretization using the Q_2/P_1^{disc} pair of finite element spaces, i.e. the velocity is approximated by continuous piecewise biquadratics in 2-D (triquadratics in 3-D) and the pressure by discontinuous linears. This conforming pair of finite element spaces fulfills the inf–sup or Babuška–Brezzi stability condition. It is currently considered among the most stable and best performing elements for finite element discretizations of Navier–Stokes equations, e.g.

see References [22, 23] or the studies in References [24, 25]. The implementation of the slip with friction boundary condition into a finite element code is described in detail in Reference [19].

The computations were performed with the code MooNMD [26, 27].

3. THE TEST PROBLEMS

The forward–backward step is one of many test problems used in computational studies. The most popular of these is the driven cavity problem. This problem is defined on a square. On all walls except the top, the no-slip condition is imposed strongly, while for the top wall the tangential component of the velocity is set to be a constant. One of the challenges posed by the driven cavity problem is the presence of non-physical singularities at the corners of the domain. However, the driven cavity problem has one major drawback in that it has no physical realization. Another commonly used test problem is the backward-facing step. In that regard, the work of Armaly *et al.* [28] stands out. The backward-facing step is a less challenging test problem since certain characteristics, i.e. the reattachment length, scale with the Reynolds number (see Reference [29]). As Gunzburger [2, p. 236] states, the forward-facing step and the full step are better test problems for computational studies since they are geometrically simple and do not scale with the Reynolds number. Concerning numerical studies of 2-D flows across a full step, stationary flows are investigated, e.g. in References [30–32]. In the 3-D regime, a closely related problem to the flow across a full step is the flow past a wall-mounted cube. The flow fields in both examples possess common features. Turbulent flows past a wall-mounted cube have been simulated, e.g. in References [33–35].

The Reynolds number in the dimensionless Navier–Stokes equations for the full step is defined by the free-stream velocity, the height of the step and the kinematic viscosity of the fluid.

3.1. The two-dimensional flow across a step

The domain of the 2-D flow across a full step that was used in our computations is presented in Figure 1. It is the same domain as in Reference [32]. On Γ_{diri}, the inflow boundary condition $\mathbf{u} = (1,0)^{\text{T}}$ is prescribed. On the top wall, a free-slip boundary condition is given ($\beta \rightarrow 0$ in (1)). Slip with friction and no penetration boundary conditions are prescribed on all lower
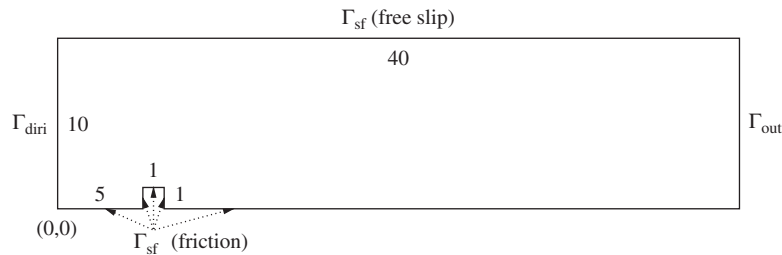

Figure 1. Two-dimensional channel with a step.

walls with the same friction parameter β. The flow leaves the domain by an outflow boundary condition on the right side of the channel.

We are interested in studying the evolution of the reattachment points of the recirculating vortices which develop behind the step. The end of the step is at the position $x = 6$. Since the tangential velocity on the bottom boundary does not vanish due to the slip with friction boundary condition, the reattachment point is given by the change of the sign of the tangential velocity. Left of the reattachment point, the tangential velocity is negative because of the recirculation of the vortex and right of the reattachment point it is positive.

We consider the flow across a full step for $Re = 500$ in the time interval $[0, 100]$. This interval was discretized with equidistant time steps of length 0.1. As initial condition, an impulsive start was used, i.e. the initial discrete velocity was chosen to be zero on all degrees of freedom (d.o.f.) which are not on the inflow boundary. The d.o.f. on Γ_{diri} were given by the inflow boundary condition. Thus, the flow needs a while for developing its characteristics and we will present results for times $t \geqslant 10$.

The initial grid (level 0) presented in Figure 2 was used to generate the computational grids employed in the numerical studies. The horizontal grid lines are placed at $y \in \{1, 2.5, 5\}$ and the vertical grid lines at $x \in \{5/3, 10/3, 5, 6, 7.785, 10.25, 14.5, 18.75, 23, 27.25, 31.5, 35.75\}$. A grid refinement is achieved by dividing each rectangle into four equal sized smaller rectangles. We will present computational results on levels 3, 4 and 5. The resulting d.o.f. are given in Table I.

Remark 1
Numerical studies of the slip with friction boundary conditions for a stationary 2-D flow across a step and a constant inflow profile were performed for $Re = 50$ and 100, see Reference [19]. In both cases, the position of the reattachment point of the recirculating vortex moved farther downstream with decreasing friction. There was a wide range of the friction parameter ($\beta \geqslant 10$) where the reattachment points differed very little from the reattachment point obtained with the no-slip boundary condition. For this boundary condition, the positions were around
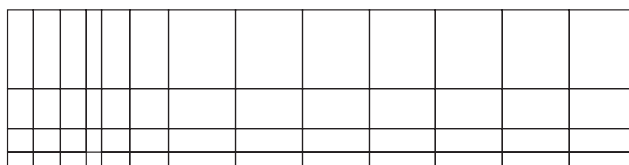

Figure 2. Two-dimensional channel with a step, coarsest grid (level 0).

Table I. Degrees of freedom for the two-dimensional flow across a step.

	Velocity	Pressure
Level 3	26 690	9 792
Level 4	105 602	39 168
Level 5	420 098	156 672

$x = 14.25$ for $Re = 50$ and $x = 20$ for $Re = 100$. For small friction, $\beta \leqslant 1$, a rapid movement of the position of the reattachment point towards the outflow boundary was observed.

3.2. The three-dimensional flow across a step

The numerical studies for the 3-D flow across a full step were performed for $Re = 200$ and final time $T = 50$. The time interval was divided in equidistant time steps of length 0.25. The initial condition was the flow field of the stationary Navier–Stokes equations with $Re = 10$.

The domain as well as the boundary conditions in these tests are given in Figure 3. We applied free-slip boundary conditions at the upper wall and no-slip boundary conditions on the left and right wall. On the lower walls, slip with friction and no penetration boundary conditions were prescribed. The constant inflow profile $\mathbf{u} = (1, 0, 0)^{\mathrm{T}}$ was used in the computations.

The initial grid is generated by the so-called sandwich grid technique. The grid presented in Figure 2 can be seen on the left and the right wall of the domain; in between there are five equal sized layers of mesh cells leading to an initial grid consisting of hexahedra. A grid refinement is performed by dividing each hexahedron into eight equal sized hexahedra. The computational results presented in this paper have been computed on level 2 (419 307 velocity d.o.f., 65 280 pressure d.o.f.) and on level 3 (3 765 075 velocity d.o.f., 522 240 pressure d.o.f.).

Remark 2

In Reference [19], numerical studies for a stationary 3-D flow across a step with $Re = 20$ and slip with friction boundary conditions can be found. The recirculating vortex defines a reattachment line. The reattachment line moved closer to the step with increasing friction. Almost the same results were obtained for applying no-slip boundary conditions and for $\beta \geqslant 0.5$. For smaller friction ($\beta \leqslant 0.1$), the reattachment line moves considerably towards the outflow. The reattachment lines were found to be symmetric for $z = 5$.
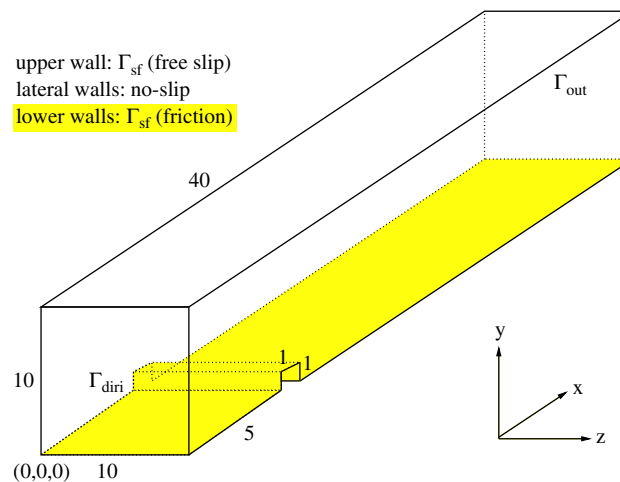

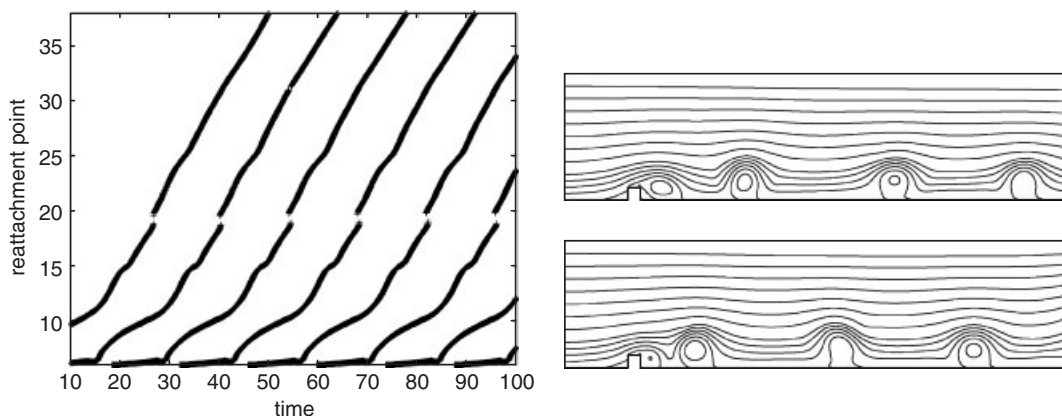Figure 3. Three-dimensional channel with a step.

4. TWO-DIMENSIONAL FLOW ACROSS A STEP AT $Re = 500$

The numerical studies were performed on the grid levels 3, 4 and 5. For the coarser grids, only a few results are presented (Table II) whereas the results on the finer grids are shown in more detail (Table II, Figures 4–9). The friction parameter β is successively set to lower values, thereby decreasing the friction on the lower part of the boundary. The values of β that were tested where $\beta \in \{10, 1, 0.5, 0.25, 0.1, 0.05, 0.01, 0.005, 0.001, 0.0001\}$. For brevity, the results for $\beta \in \{10, 0.5, 0.25, 0.0001\}$ are not shown explicitly. The results for $\beta = 10$ agree quantitatively and qualitatively with the results for $\beta = 1$, the results for $\beta \in \{0.5, 0.25\}$ look similar to the results for $\beta \in \{1, 0.1\}$ and the results for $\beta = 0.0001$ agree with the results for $\beta = 0.001$.

For $\beta \in \{1, \ldots, 0.05\}$, we observe that the flow is periodic: vortices are formed behind the step and then shed during regular time intervals. The lengths of the periods on different levels of the grid refinement, averaged in the time interval $[10, 100]$, are given in Table II. The flow is reminiscent of the top half of the flow of a viscous fluid past a cylinder. At first sight, and for the aforementioned values of β, the flow seems to exhibit the same quantitative and qualitative behaviour. However, for all grids which were involved in our numerical studies, *as the friction parameter decreases*, *the length of the period shows a small increase*, see Table II.

Table II. Averaged length of the period of the vortex shedding.

β	10	1	0.5	0.25	0.1	0.05
Level 3	13.75	13.83	13.90	14.04	14.31	14.35
Level 4	13.81	13.86	13.90	13.98	14.24	14.47
Level 5	13.77	13.82	13.86	13.94	14.27	14.51

Figure 4. Two-dimensional flow across a step at $Re = 500$, $\beta = 1$, evolution of reattachment points and streamlines at $t = 50$ and 100 s, level 5.
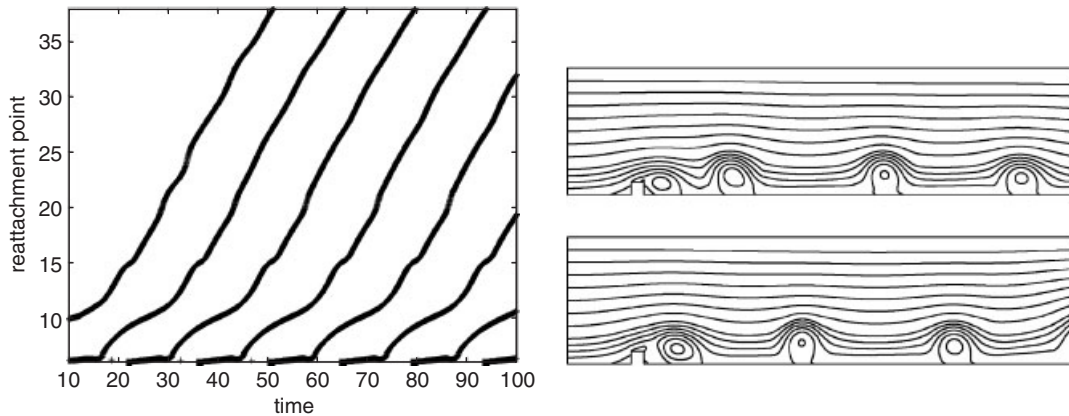
Figure 5. Two-dimensional flow across a step at $Re = 500$, $\beta = 0.1$, evolution of reattachment points and streamlines at $t = 50$ and 100 s, level 5.
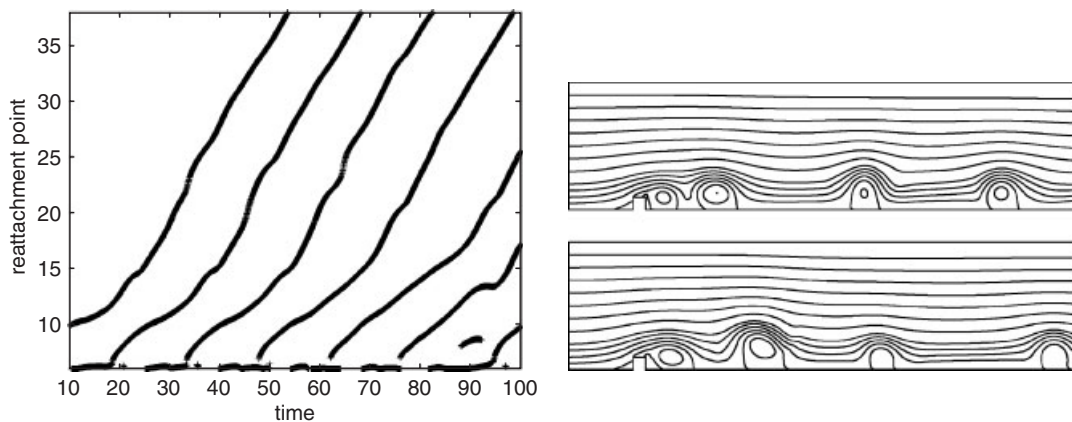

Figure 6. Two-dimensional flow across a step at $Re = 500$, $\beta = 0.05$, evolution of reattachment points and streamlines at $t = 50$ and 100 s, level 5.

For $\beta = 1$, it can be observed that the vortex separates from the lower boundary at x around 20 and starts to attach a little bit farther downstream again. This is the reason of the discontinuity of the curves in Figure 4.

For $\beta = 0.01$, vortex shedding can still be observed with two major changes occurring. First, *the reattachment point moves at a much slower rate*; second, *the vortices behind the step are significantly larger in size*. For $\beta \leqslant 0.005$, *the flow abruptly ceases to be periodic* (at least for the given time interval). The reattachment point continues to move downstream, however, there is no vortex shedding observed.
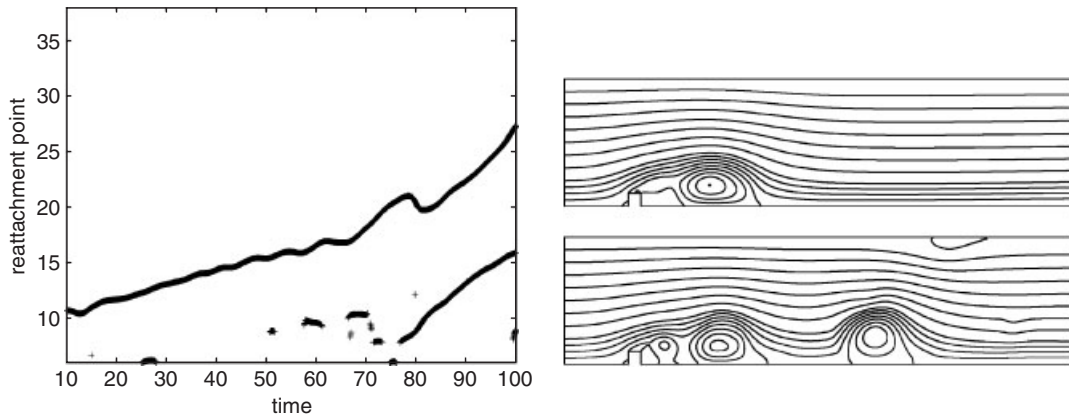
Figure 7. Two-dimensional flow across a step at $Re = 500$, $\beta = 0.01$, evolution of reattachment points and streamlines at $t = 50$ and 100 s, level 5.
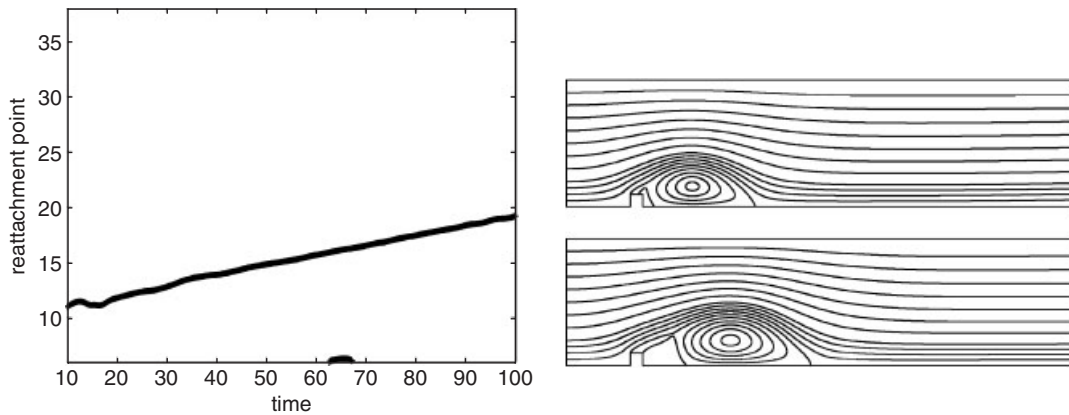

Figure 8. Two-dimensional flow across a step at $Re = 500$, $\beta = 0.005$, evolution of reattachment points and streamlines at $t = 50$ and 100 s, level 5.

In order to explain the variations in the shedding of vortices, we must first concentrate on the reasons of boundary layer separation. Since the boundary condition on the upper part of the boundary is free slip, vorticity and viscous forces are confined to a thin boundary layer on the lower part of the boundary. There, the second component of the velocity $\mathbf{u} = (u, v)$ is very small such that its role in the momentum equation can be neglected and the first momentum equation reduces to

$$\frac{\mathrm{D}u}{\mathrm{D}t} := u_t - 2Re^{-1}\left(\frac{\partial^2 u}{\partial x^2} + \frac{1}{2}\frac{\partial^2 u}{\partial y^2}\right) + u\frac{\partial u}{\partial x} = -\frac{\partial p}{\partial x}$$
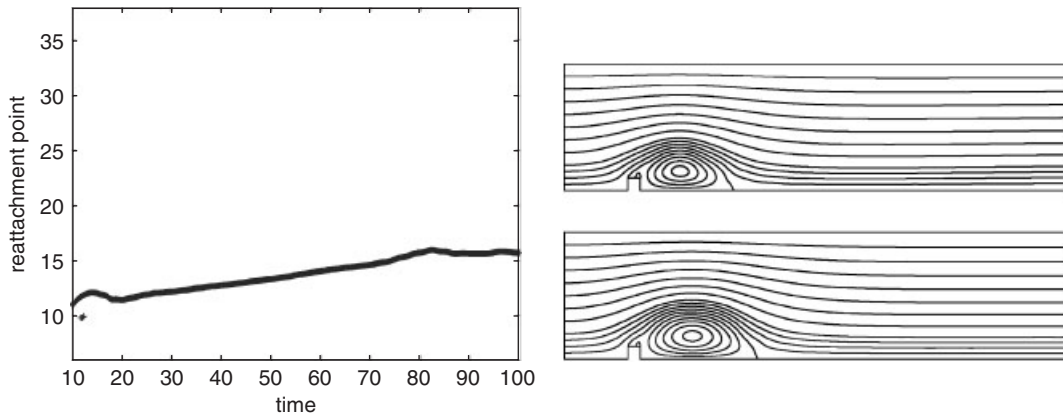
Figure 9. Two-dimensional flow across a step at $Re = 500$, $\beta = 0.001$, evolution of reattachment points and streamlines at $t = 50$ and 100 s, level 5.

where Du/Dt is the substantive derivative. Assuming for simplicity that at $y = 0$ the fluid is inviscid, which is justified for large Re, the above equation reduces to

$$u_t + u\frac{\partial u}{\partial x} = -\frac{\partial p}{\partial x}$$

The above equation could also be derived by Bernoulli's streamline theorem. Clearly, any increase in u results in a decrease in p and *vice versa*.

Getting back to our problem, we see that the fluid has to speed up to go past the step thus the tangential component of the velocity on top of the step is large. Consequently, the pressure must be small. In addition, the pressure is large at the stagnation points directly in front and behind the step where the velocity is small. The increase in pressure in the direction of the flow (adverse pressure gradient) causes reversed flow close to the boundary where the fluid moves slower due to the boundary condition; in turn, this leads to the separation of the boundary layer.

The reason why vortices are being shed up to a certain coefficient of friction is due to two critical factors; the vorticity (i.e. circulation) behind the step and the friction itself. The primary cause of vorticity behind the step is friction. The kinetic energy loss due to friction is recovered in the rotational kinetic energy of the eddy behind the step. Once the vorticity achieves a critical value, the eddy 'rolls' downstream, much in the same fashion as a ball being swept by the current. Friction here works as the force that helps the vortex move downstream; the fluid in the vortex cannot slip past the wall thus the eddy 'rolls' downstream on the bottom of the channel. When the friction coefficient is lowered, the fluid can slip, and thus the eddy can remain behind the step longer. This is clearly seen in our numerical simulations since with lower friction coefficients, the reattachment point moves slower. In addition, as the eddy remains behind the step longer, more vorticity is fed into the eddy thus the eddy becomes larger and 'rolls' downstream with lower speed. Naturally, the mechanism of formation of vortices via the detachment of boundary layers continues so another vortex

will form and the cycle will continue. Finally, there is no eddy dissipation observed as the kinematic viscosity is very low.

5. THREE-DIMENSIONAL FLOW ACROSS A STEP AT $Re = 200$

Results of the numerical simulations are shown in Figures 10–14. For the friction parameter β, we used the values $\beta \in \{10, 1, 0.1, 0.01, 0.001\}$. The results for $\beta = 0.1$ are not presented
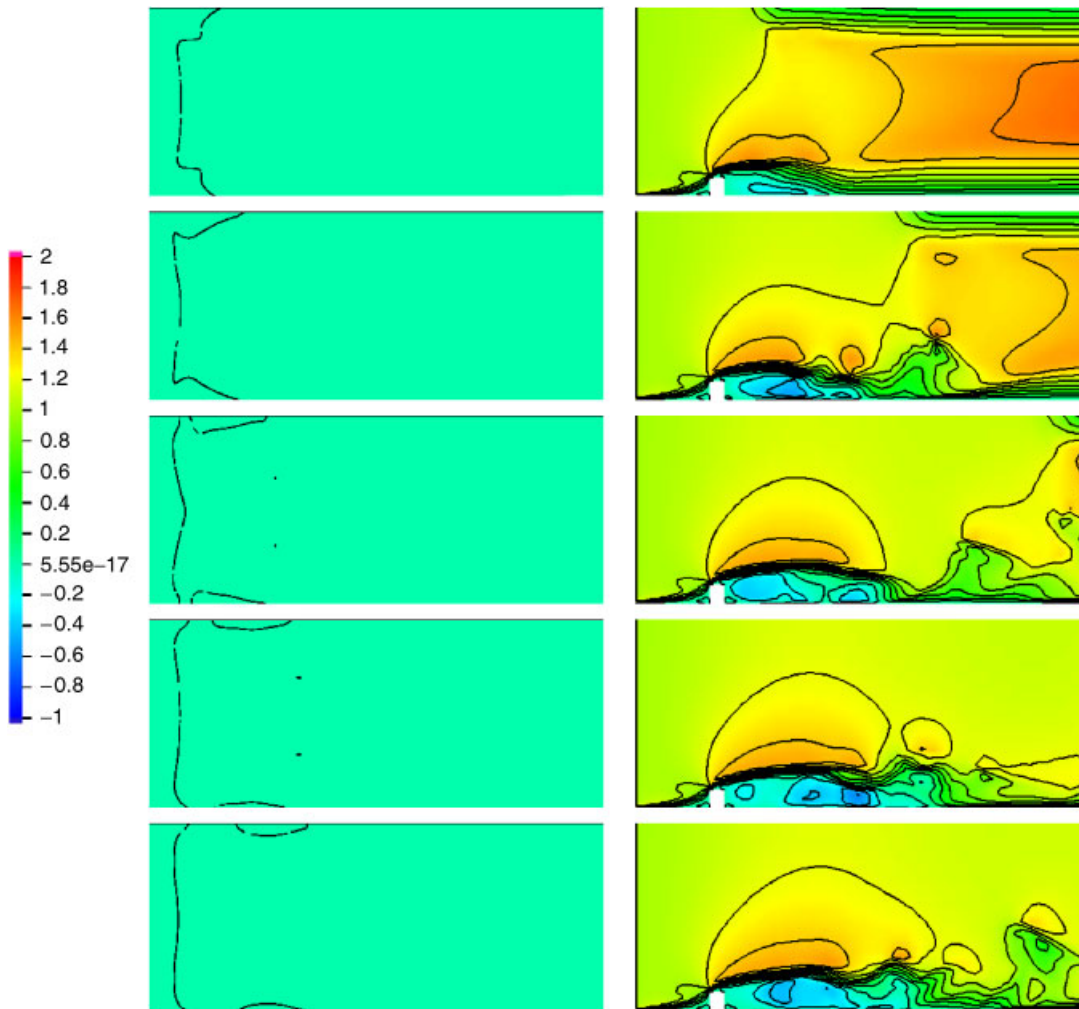

Figure 10. Three-dimensional flow across a step at $Re = 200$, isolines on the bottom of the channel $y = 0, x \geqslant 6$ (left) and on the centre plane $z = 5$ of the first velocity component (right) for the times $t = 10, 20, 30, 40$ and 50 s (top to bottom) and the friction parameter $\beta = 10$, level 3.

Figure 11. Three-dimensional flow across a step at $Re = 200$, isolines on the bottom of the channel $y = 0, x \geqslant 6$ (left) and on the centre plane $z = 5$ of the first velocity component (right) for the times $t = 10, 20, 30, 40$ and 50 s (top to bottom) and the friction parameter $\beta = 1$, level 3.
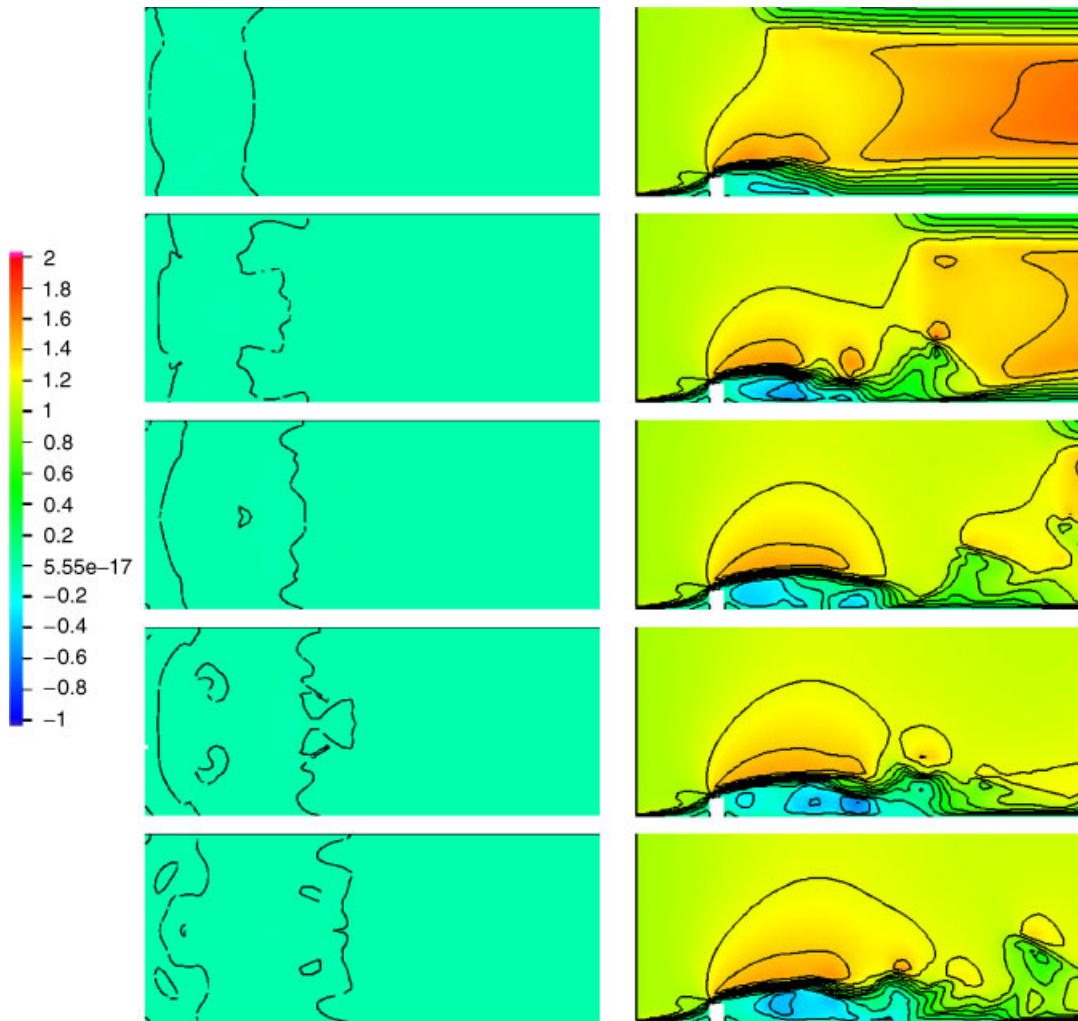
since they agree quantitatively and qualitatively with the results for $\beta = 1$. We will see that the results of the 3-D flow across a full step differ in many respects from the results of the 2-D flow across a full step, Section 4, since the physics of the flow is different.

In Figures 10–14, we present *isolines of the first velocity component* on the bottom of the channel immediately after the step, without including the step. The isolines range from -1 (backward flow, dark regions) to 2 (forward flow, light regions) and their distance is 0.2. The colour for the value 0 can be observed best in Figure 10 since, for this friction parameter, the fluid almost sticks to the bottom of the channel. Beside the bottom of the channel, we
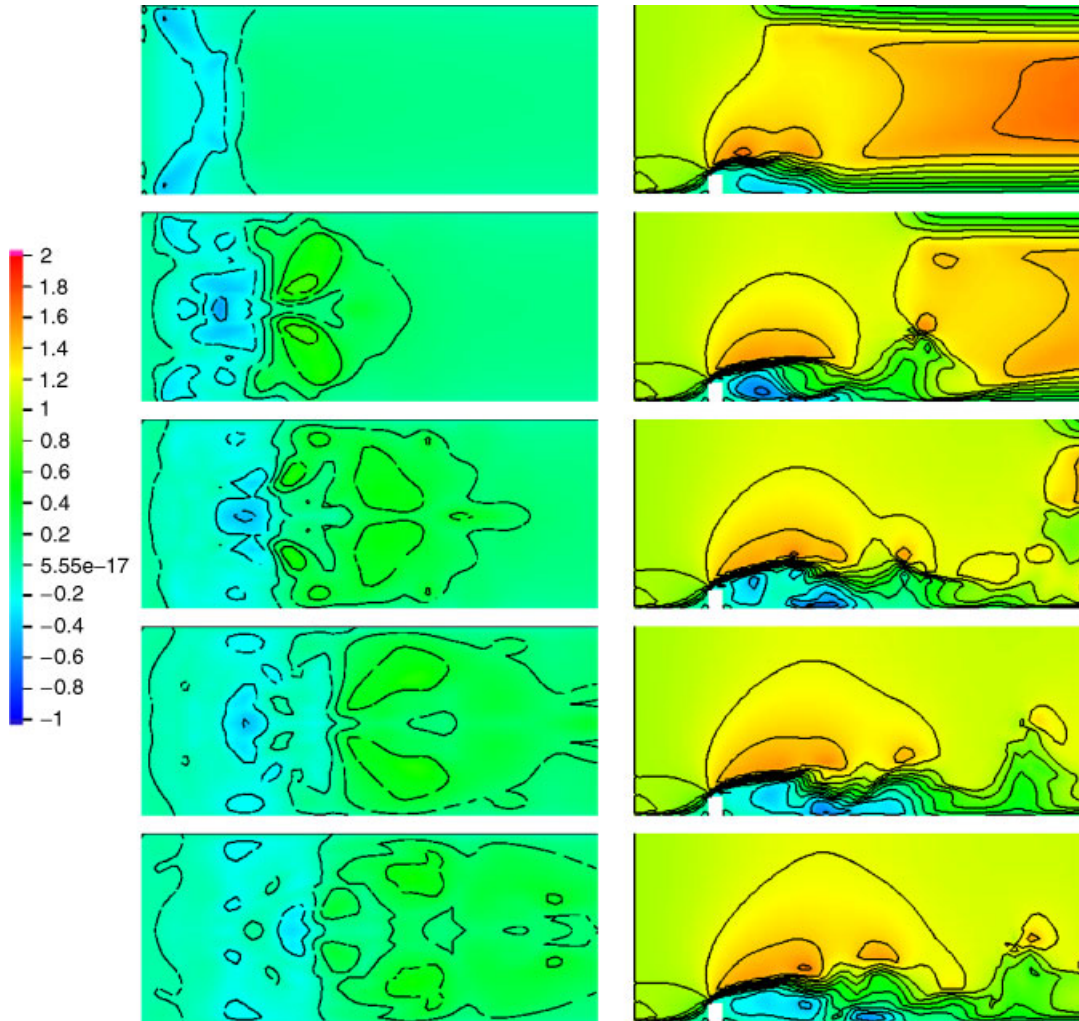
Figure 12. Three-dimensional flow across a step at $Re = 200$, isolines on the bottom of the channel $y = 0, x \geqslant 6$ (left) and on the centre plane $z = 5$ of the first velocity component (right) for the times $t = 10, \ 20, \ 30, \ 40$ and $50 \, \text{s}$ (top to bottom) and the friction parameter $\beta = 0.01$, level 3.

present also the isolines of the first velocity component in the central cut plane $z = 5$. In the evaluation of the results in this plane, we are interested in the vortices which are near the bottom behind the step.

Again, we will study the results on the finest computational grid in detail, Figures 10–13, and present only a few results on the coarser grid, Figure 14. Figure 14 shows that at the final time $t = 50 \, \text{s}$ we get qualitative agreement between the results obtained on the coarse and fine grids.
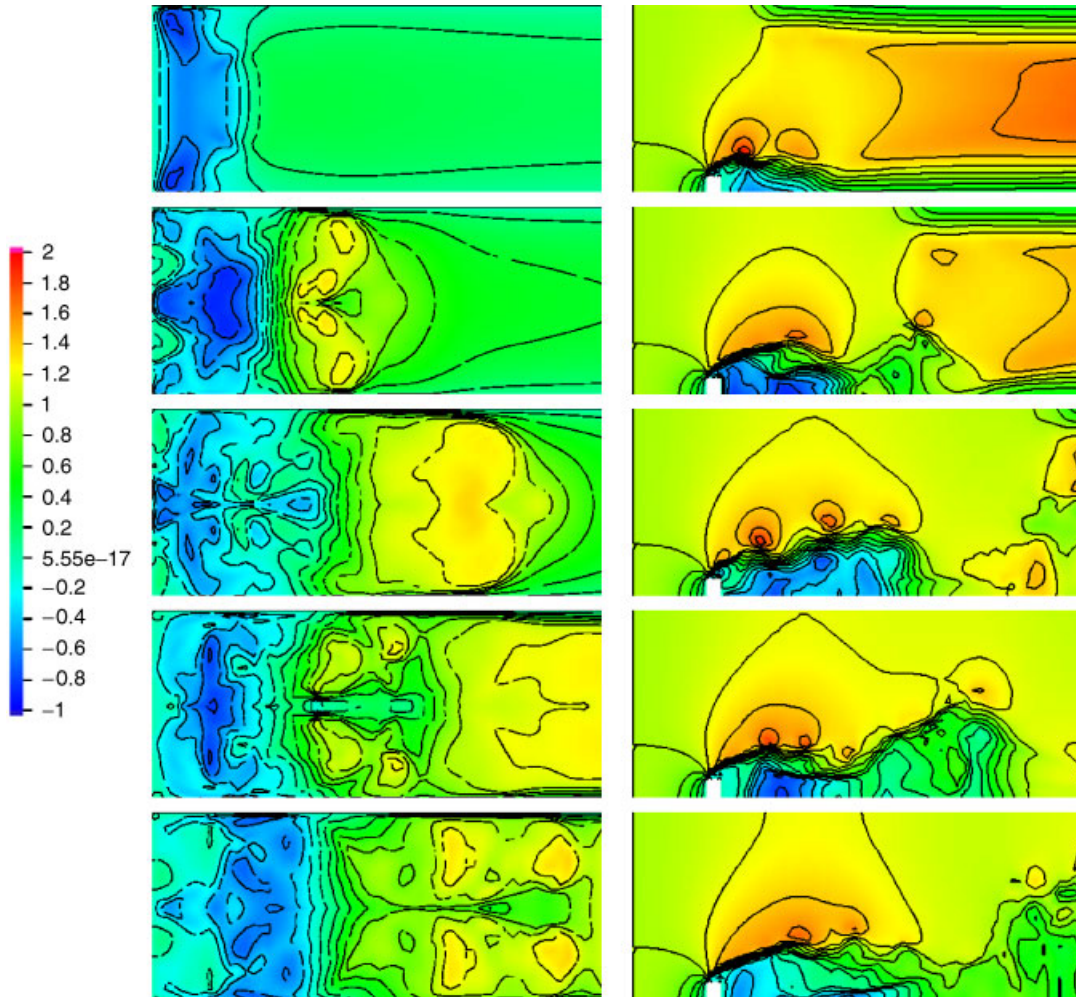
Figure 13. Three-dimensional flow across a step at $Re = 200$, isolines on the bottom of the channel $y = 0, x \geqslant 6$ (left) and on the centre plane $z = 5$ of the first velocity component (right) for the times $t = 10$, 20, 30, 40 and 50 s (top to bottom) and the friction parameter $\beta = 0.001$, level 3.

There are major differences between the flow for $\beta = 10$ and the flows for the remaining choices for β. Let us first concentrate on the bottom of the channel. Note that for $\beta = 10$ the isolines correspond to $u = 0$ so we can refer to them as reattachment curves. The reattachment curves remain for the most part stationary with only the parts near the left and right walls stretching and detaching. For lower values of β, the morphology of the flow changes dramatically. While for $\beta = 10$, the reattachment curves are isolated along the lateral walls, for $\beta < 10$, the isolines on the bottom of the channel spread all across the bottom boundary. Looking at averages of the isolines corresponding to $u = 0$, we note that the period of vortex
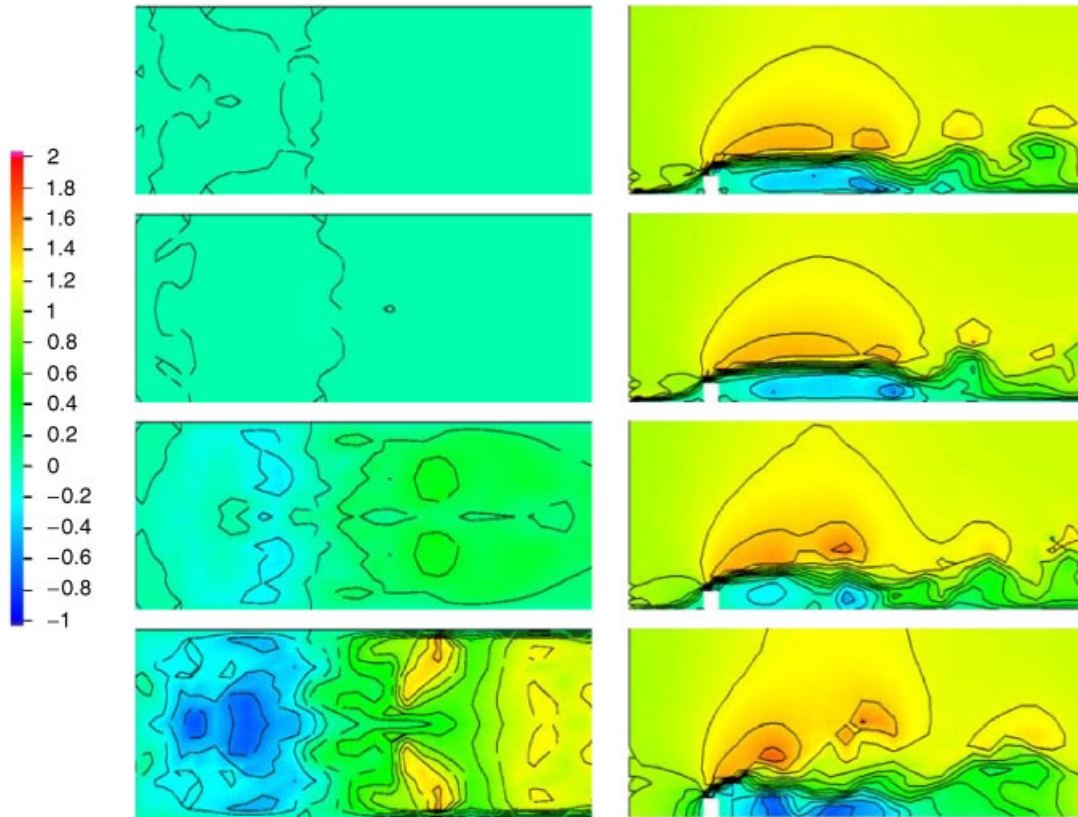
Figure 14. Three-dimensional flow across a step at $Re = 200$, isolines on the bottom of the channel $y = 0, x \geqslant 6$ (left) and on the centre plane $z = 5$ of the first velocity component (right) for the time $t = 50$ s, friction parameter $\beta = 10, \beta = 1, \beta = 0.01, \beta = 0.001$ (top to bottom), level 2.

shedding is increasing slightly. In addition, for $\beta < 1$, we observe, as expected, a range of boundary velocities. Specifically, for $\beta = 0.001$, the eddy behind the step seems to be getting stronger, based on the dark colouring of the regions inside the isolines. Finally, we see a resemblance to 2-D flow in the sense that the eddy behind the step persists for longer times and is larger in size since the dark regions become larger. We note that for $\beta = 10$ a slight difference can be observed between the results on the coarse and the fine grid. On the coarse grid, there are additional reattachment lines in the centre of the channel besides the characteristic reattachment lines at the lateral walls.

Turning our attention to the centre plane view of the channel, we note that for all β there is a large eddy which forms behind the step, which contains smaller eddies that seem to move within it and 'coalesce' into larger eddies, see time 30, 40 and 50 s. The flows for $\beta = 10$ and 1 seem similar. Comparing the centre plane view with the bottom wall view, we observe that the recirculating eddies seem to glide along the bottom boundary since there is no trace of these eddies along the bottom wall, i.e. there is no isoline where the first velocity component

is zero (reattachment line). In all cases, the flow looks quite different from the 2-D flows presented in Section 4.

The explanation of the results is based upon the *vorticity transport equation* for incompressible flow (obtained by taking the curl of the Navier–Stokes equations):

$$\frac{\partial \boldsymbol{\omega}}{\partial t} + (\mathbf{u} \cdot \nabla)\boldsymbol{\omega} = (\boldsymbol{\omega} \cdot \boldsymbol{\nabla})\mathbf{u} + Re^{-1}\Delta\boldsymbol{\omega} \tag{2}$$

where $\boldsymbol{\omega} = \nabla \times \mathbf{u}$ is the vorticity, and $\mathbf{u} = (u, v, w)$ is the fluid velocity. Equation (2) tells us that the rate of change of the vorticity as it moves along with the fluid is dependent on two factors: the stretching and tilting of vortex filaments due to velocity gradients, $(\boldsymbol{\omega} \cdot \boldsymbol{\nabla})\mathbf{u}$, and the diffusion of vorticity due to the viscosity of the fluid, $Re^{-1}\Delta\boldsymbol{\omega}$. Diffusion of vorticity affects primarily the small eddies (see Reference [36, Section 34]). This is readily observed in the figures for $\beta < 10$, where small eddies are diffused into the flow. In comparison to the smooth flow fields in the 2-D simulations, all 3-D flow fields contain significantly more eddies. The flow fields in 3-D are much more complex despite the low Reynolds number.

For $\beta = 10$, vorticity is produced at the left/right corners right after the step as the flow proceeds. There, and in contrast with the rest of the flow, the fluid is in contact with 3 surfaces (lateral wall, step wall and bottom wall) where the friction coefficient is high. As the production of vorticity at the corners $(6, 0, 0)$ and $(6, 0, 10)$ is higher than at any other point behind the step, the vortex filament stretches there more than in any other location. In addition, the velocity gradients, specifically $\partial u/\partial z$ at or near the bottom, are not sufficient to force the vortex to tilt and stretch along the z-direction. Once the vortex reaches a certain size or when a critical value of the circulation is achieved, the vortex, with the aid of friction rolls along the lateral and lower walls. For all friction parameters, the leading edge of the vortex behind the step, other than at the left/right corners, is observed in general at $z = 5$ since the velocity obtains a maximum there. Decreasing the friction coefficient allows the velocity at the bottom wall to increase. Production of vorticity still occurs at the lateral walls, with the difference that now the component $\partial u/\partial z$ of the velocity gradient dominates which stretches and tilts the vortex. This is exactly what is observed in our results.

Turning our attention once more to the central plane view of the channel, we note that the cease of 'gliding' of the eddies behind the step is caused by the thinning of the boundary layer due to the decrease of friction. This has a dual effect: not only that for large values of β all eddies must glide along the boundary but also that the period of eddy shedding is smaller. For lower values of β we observe the same phenomenon as in the 2-D case: because of lack of friction, all the vorticity generated moves toward the outflow with a slower pace. As a result, the eddy behind the step becomes stronger, however, without significant changes in size *on the plane of view*. However, if we combine the perspective of the bottom wall view, we see that the recirculating eddy tilts and stretches as predicted by the vorticity transport equation.

6. SUMMARY

Numerical results for the time-dependent 2-D and 3-D flow of a Newtonian fluid over a full step with slip with friction boundary conditions and Reynolds numbers 500 and 200, respectively, were presented. In both cases, recirculating eddies formed behind the step which

were periodically shed with decreasing period as the coefficient of friction $\beta \to 0$. In the 2-D case and as the friction coefficient was decreased, the size of the recirculating eddy increased and the periodic shedding ceased as β reached a critical value. While the flow in the 3-D case had common characteristics with the 2-D flow (periodic vortex shedding), it was more complicated and offered more insight into the motion of vortices.

As exhibited by the vorticity transport equation, (2), vortices are not only subject to translations (as in the 2-D case). They diffuse into the flow and stretch and tilt according to velocity gradients which change on the boundary when the coefficient of friction is altered. Centre plane views in combination with bottom wall views of all flows exhibit this motion. All numerical simulations are in agreement with the physics of the flow.

REFERENCES

1. Galdi GP. Introduction to the mathematical theory of the Navier–Stokes equations. *Volume 1 of Tracts in Natural Philosophy*, vol. 38, revised edition. Springer: Berlin, 1998.
2. Gunzburger MD. *Finite Element Methods for Viscous Incompressible Flows*: *A Guide to Theory*, *Practice*, *and Algorithms*. Academic Press: New York, 1989.
3. Girault V, Raviart PA. Finite element approximation of the Navier–Stokes equations. *Volume v.749 of Lecture Notes in Mathematics*. Springer: Berlin, 1979.
4. Day MA. The no-slip condition of fluid dynamics. *Erkenntnis* 1990; **33**:285–286.
5. LeRoux C. Second grade fluids with slip boundary conditions. *Ph.D. Thesis*, University of Pretoria, Pretoria, South Africa, May 1997.
6. Kundt A, Warburg E. On friction and thermal conductivity in rarefied gases. *Philosophical Magazine* 1875; **50**:53.
7. Maxwell JC. On the condition to be satisfied by a gas at the surface of a solid body. *Scientific Papers* 1879; **2**:704.
8. Petroff N. *A New Theory of Friction*, volume Bd. 218. Ostwald's Klassiker, 2000. Originally published 1927.
9. Galdi GP, Layton WJ. Approximation of the larger eddies in fluid motion II: a model for space filtered flow. *Mathematical Models and Methods in Applied Sciences* 2000; **10**(3):343–350.
10. Navier CMLH. Sur les lois de l'equilibre et du mouvement des corps élastiques. *Memoires de l'Academie des Sciences de l'Institut de France* 1827; **6**:389–441.
11. Serrin J. Mathematical principles of classical fluid mechanics. *Encyclopedia of Physics*, vol. VIII/1. Springer: Berlin, 1959; 125–263.
12. Duhem P. On the boundary conditions in hydrodynamics. *Comptes Rendus* 1902; **134**:149–151.
13. Duhem P. On certain cases of adherence of a viscous liquid to solids immersed in it. *Comptes Rendus* 1902; **134**:265–267.
14. Oseen CW. Contributions to hydrodynamics. *Annalen der Physik* 1915; **46**:231–252, 623–640.
15. Noaillon P. Attempt at a new theory of the resistance of fluids. *Comptes Rendus* 1929; **188**:441–443.
16. Clopeau T, Mikelic A, Robert R. On the vanishing viscosity limit for the 2D incompressible Navier–Stokes equations with the friction type boundary conditions. *Nonlinearity* 1998; **11**(6):1625–1636.
17. Coron JM. On the controllability of the 2-D incompressible Navier–Stokes equations with the Navier slip boundary conditions. *ESAIM Contrôle Optimisation and Calculus of Variations* 1996; **1**:35–75.
18. Hwang RR, Chow YC, Peng YF. Numerical study of turbulent flow over two-dimensional surface-mounted ribs in a channel. *International Journal for Numerical Methods in Fluids* 1999; **31**:767–785.
19. John V. Slip with friction and penetration with resistance boundary conditions for the Navier–Stokes equations—numerical tests and aspects of the implementation. *Journal of Computational and Applied Mathematics* 2002; **147**:287–300.
20. Pope SB. *Turbulent Flows*. Cambridge University Press: Cambridge, MA, 2000.
21. John V, Layton WJ, Sahin N. Derivation and analysis of near wall models for channel and recirculating flows. *Computers and Mathematics with Applications* 2004; **48**:1135–1151.
22. Fortin M. Finite element solution of the Navier–Stokes equations. In *Acta Numerica*, Iserles A (ed.). Cambridge University Press: Cambridge, MA, 1993; 239–284.
23. Gresho PM, Sani RL. *Incompressible Flow and the Finite Element Method*. Wiley: New York, 1998.
24. John V, Matthies G. Higher order finite element discretizations in a benchmark problem for incompressible flows. *International Journal for Numerical Methods in Fluids* 2001; **37**:885–903.
25. John V. Higher order finite element methods and multigrid solvers in a benchmark problem for the 3D Navier–Stokes equations. *International Journal for Numerical Methods in Fluids* 2002; **40**:775–798.

26. John V. Large eddy simulation of turbulent incompressible flows. Analytical and numerical results for a class of LES models. *Volume 34 of Lecture Notes in Computational Science and Engineering*. Springer: Berlin, Heidelberg, New York, 2004.
27. John V, Matthies G. MooNMD—a program package based on mapped finite element methods. *Computer Visual Sciences* 2004; **6**:163–170.
28. Armaly BF, Durst F, Pereira JCF, Schoenung B. Experimental and theoretical investigation of backward-facing step flow. *Journal of Fluid Mechanics* 1983; **127**:473–496.
29. Halim A, Hafez M. Calculation of separation bubbles using boundary layer type equations. *Computational Methods in Viscous Flows*, vol. 3. Pineridge Press: Swansea, 1984; 395–415.
30. Gresho PM, Lee RL. Don't suppress the wiggles–they're telling you something. *Computers and Fluids* 1981; **9**:223–253.
31. Gresho PM, Leone JM. Finite element simulations of steady two-dimensional, viscous incompressible flow over a step. *Journal of Computational Physics* 1981; **41**(1):167–191.
32. Fragos VP, Psychoudaki SP, Malamataris NA. Computer-aided analysis of flow past a surface-mounted obstacle. *International Journal for Numerical Methods in Fluids* 1997; **25**:495–512.
33. Shah KB. Large eddy simulation of the flow past a cubic obstacle. *Ph.D. Thesis*, Stanford University, 1998.
34. Rodi W, Ferziger JH, Breuer M, Pourquie M. Status of large eddy simulation: result of a workshop. *Journal of Fluids Engineering* 1997; **119**:248–262.
35. Ooia A, Iaccarinob G, Durbinc PA, Behniad M. Simulation of turbulent flow and heat transfer in complex passages. Under consideration for publication in *International Journal of Heat and Fluid Flow*. Found in `http://ctr-sgi4.stanford.edu/~gianluca/pdf/ijhff.pdf`
36. Landau LD, Lifshitz EM. Fluid mechanics. *Course of Theoretical Physics*, vol. 6. Addison-Wesley: Reading, MA, 1959.